Chemistry & Biology *13*, 81–90, January 2006 DOI 10.1016/j.chembiol.2005.10.014

Target Structure-Based Discovery of Small Molecules that Block Human p53 and CREB Binding Protein Association

Sachchidanand,[1] Lois Resnick-Silverman,[2] Sherry Yan,[1] Shiraz Mutjaba,[1] Wen-jun Liu,[2] Lei Zeng,[1] James J. Manfredi,[2] and Ming-Ming Zhou[1,*]
[1]Structural Biology Program
Department of Physiology and Biophysics
[2]Department of Oncological Sciences
Mount Sinai School of Medicine
New York University
1425 Madison Avenue
New York, New York 10029

Summary

Lysine acetylation of human tumor suppressor p53 in response to cellular stress signals is required for its function as a transcription factor that regulates cell cycle arrest, senescence, or apoptosis. Here, we report small molecules that block lysine 382-acetylated p53 association with the bromodomain of the coactivator CBP, an interaction essential for p53-induced transcription of the cell cycle inhibitor p21 in response to DNA damage. These chemicals were discovered in target structure-guided nuclear magnetic resonance spectroscopy screening of a focused chemical library constructed based on the structural knowledge of CBP bromodomain/p53-AcK382 binding. Structural characterization shows that these chemicals inhibit CBP/p53 association by binding to the acetyl-lysine binding site of the bromodomain. Cell-based functional assays demonstrate that the lead chemicals can modulate p53 stability and function in response to DNA damage.

Introduction

The human tumor suppressor p53 is a transcription factor that binds in a sequence-specific manner to particular sites in the genome and activates transcription of target genes [1–3]. It plays a pivotal role in cellular response to stress signals in cell cycle arrest, senescence, DNA repair, or apoptosis [4–7]. The biological activity of p53 is tightly regulated by posttranslational modifications in its N- and C-terminal regions [1, 6, 8]. Upon DNA damage, p53 is extensively phosphorylated within the N-terminal activation domain, which relieves it from association with the negative regulator Mdm2, resulting in p53 stabilization and activation [9–11]. In addition, phosphorylation occurs in the C terminus of p53, which has been suggested to enhance its DNA binding in vitro [12, 13].

In response to extracellular stress or DNA damage, p53 becomes acetylated on multiple lysine residues at its C terminus [14–16]. Particularly, the transcriptional coactivator histone acetyltransferase p300/CREB binding protein (CBP) has been shown to acetylate K373, K382, and, to a lesser extent, K372 and K381, whereas another coactivator, p300/CBP-associated factor (PCAF), acetylates K320. The dynamic interplay between lysine acetylation and deacetylation of p53 has been directly linked to its ability to regulate p53 stability or protein level in cells as well as functional activation as a transcription factor in cell cycle arrest, apoptosis [17–21], and senescence [22]. It was hypothesized on the basis of in vitro data that p53 acetylation enhances its DNA binding through the relief of negative regulation of DNA binding exerted by the C-terminal region [14–16]. However, more recent cell-based studies show that lysine acetylation of p53 may not result in direct enhancement of its DNA binding ability [14–16], but rather promotes its recruitment of transcriptional coactivators, which leads to subsequent histone acetylation of chromatin and transcriptional activation of its target genes [20]. Indeed, our recent study shows that acetylated K382 in p53 serves as a binding site for the CBP bromodomain (BRD), and that this BRD/acetyl-lysine (AcK) binding is responsible for p53 acetylation-dependent coactivator recruitment after DNA damage, a step that is essential for p53-induced transcriptional activation of the cyclin-dependent kinase inhibitor p21 in G1 cell cycle arrest [23].

Despite the fact that these posttranslational modifications are known to play an important role in p53 function, specific effects of single or combinatorial modifications on p53 function remain elusive. Because many of these modifications are clustered within a relatively short stretch of the protein sequence, conventional point mutational analysis of one modification site can lead to masking of effects exerted by different neighboring modifications. To circumvent this problem, we aimed to develop small-molecule chemical ligands that are capable of selectively modulating molecular interactions and regulation of p53 function involving these modifications, particularly lysine acetylation. Such small molecules can be used to study endogenous p53 and its effector proteins in cell-based assays, which may help us gain mechanistic insights into the effects of single or combinatorial modifications on p53 activation in response to DNA damage.

In this study, we report the identification of a series of small-molecule chemical compounds that can block K382-acetylated p53 association with the BRD of CBP. These small molecules were discovered in target structure-based nuclear magnetic resonance (NMR) spectroscopy screening of a focused library of chemical compounds that was constructed based on the structural knowledge of the CBP BRD/p53-AcK382 interaction. Our structure-based characterization, using combined experimental and computational methods, shows that some of these small-molecule compounds can effectively inhibit CBP/p53 association by specifically binding to the AcK binding pocket of the CBP BRD. Cell-based functional assays further demonstrate that the lead chemicals can modulate p53 stability, protein level, and modification patterns, as well as transcriptional activation of downstream target gene p21 in response to DNA damage. The combined in vitro and in vivo studies with these small molecules also help in selection of ligand for further lead optimization.

*Correspondence: ming-ming.zhou@mssm.edu

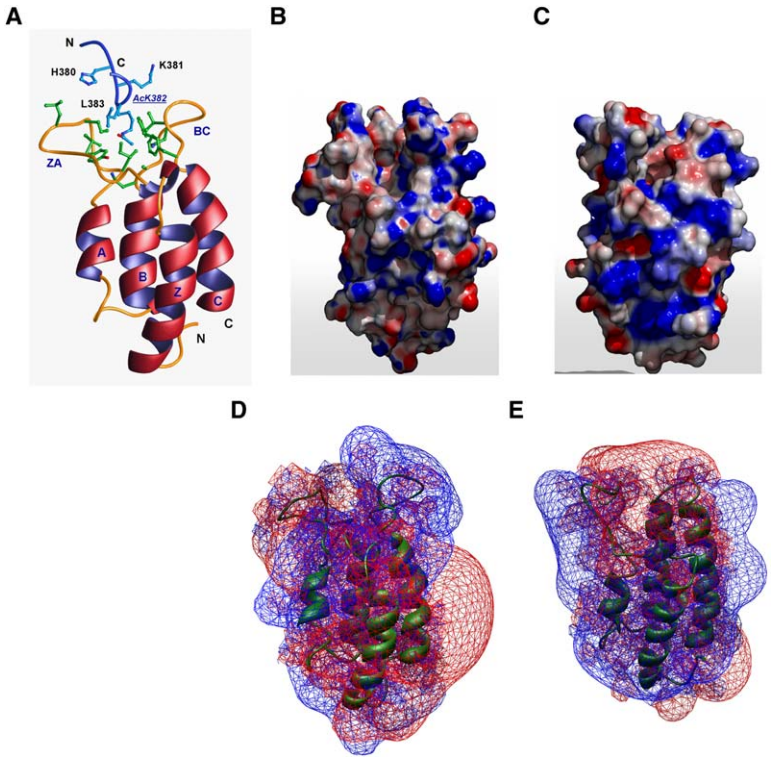

Figure 1. Physicochemical Properties of the AcK Binding Sites in the CBP and PCAF BRDs

(A) Ribbon diagram of the 3D structure of the CBP BRD in complex with lysine 382-acetylated p53 peptide (PDB 1JSP).

(B and C) Surface electrostatic potential representation of the BRDs of CBP and PCAF, respectively. The electrostatic potential of the protein molecular surface was calculated using Delphi [47], and figures were produced using GRASP [49] and rendered using Pov4Grasp (http://pov4grasp.free.fr/).

(D and E) 3D representations of electrostatic isopotential contours of the CBP and PCAF BRDs. Contours are drawn at $-1K_B/T$ (red) and $+1K_B/T$ (blue). The electrostatic potential was calculated using Delphi [47] and the figure was made using UCSF Chimera [48].

Results and Discussion

Knowledge-Based Design of a Focused Library

NMR-based screening of chemical compounds for a given target protein is considered to be reliable and target site-specific, making it preferable over random high-throughput screening [24–27]. However, because of relatively slow speed of NMR spectral acquisition and requirement of significant amount of protein samples, NMR is generally not best suited for chemical screening in a high-throughout fashion. To circumvent this shortcoming, we have employed a strategy that combines a target structural knowledge-based construction of a "focused" library and NMR screening for lead identification.

In designing a library, diversity of chemical compounds plays an important role in the successful outcome of screening [28]. Although a desirable property, chemical diversity is not the sole criterion; and pure diversity emphasis may bias libraries away from preferred drug properties [29, 30]. Need of chemical diversity coverage for successful lead identification, however, is inversely proportional to available structural and functional knowledge for a given target.

The BRD is found in a large number of chromatin-associated proteins and nuclear histone lysine acetyltransferases (HATs), and has been recently shown to function as an AcK binding domain [31]. BRD/AcK binding plays a pivotal role in regulation of chromatin remodeling and gene transcription [32, 33]. BRDs adopt a conserved structural fold of a left-handed four-helix bundle (αZ, αA, αB, and αC), as first shown in the PCAF BRD [34]. The ZA and BC loops at one end of the bundle form a hydrophobic pocket for AcK binding. The structure of the CBP BRD bound to a p53-AcK382 peptide [23] shows that AcK382 intercalates into the protein hydrophobic cavity and interacts with residues of the ZA and BC loop (Figure 1A). The structures of PCAF BRD/HIV Tat-AcK50 [35] and GCN5p BRD/H4-AcK16 [36] complexes confirm that the residues in BRDs important for AcK recognition are largely conserved, whereas sequence variations in the ZA and BC loops with amino acid deletion or insertion enable discrimination of different binding targets.

The AcK binding pocket is hydrophobic in nearly all BRDs, whereas electrostatics at the opening of the AcK binding pocket displays significant variations in different BRDs. For example, in CBP BRD, the opening is slightly positively charged, while it is more negatively charged in PCAF BRD (Figure 1B versus 1C and 1D versus 1E). These differences at the ligand binding site could serve as the basis for selectivity of chemical ligands targeting a particular BRD. Given these structural feature differences at the AcK binding pocket and the fact that most known drug molecules contain one aromatic ring, we constructed a knowledge-based library of ~200 compounds from a collection of ~14,000 small molecules (ChemBridge Corporation, San Diego, CA). The following criteria were used for the compound selection: (1) each compound consists of one aromatic ring connected to a $-NHCOCH_3$ group, either directly or via a two-three carbon chain; and (2) drug-like properties of compounds are evaluated according to the Lipinsky's Rule of Five [37].

Lead Identification by NMR

We divided the library of 200 compounds into 25 screening mixtures, with each containing eight compounds. Ligand binding to the protein was detected by monitoring chemical shift changes of protein backbone amide resonances in 2D ^{1}H-^{15}N-HSQC spectra acquired in the

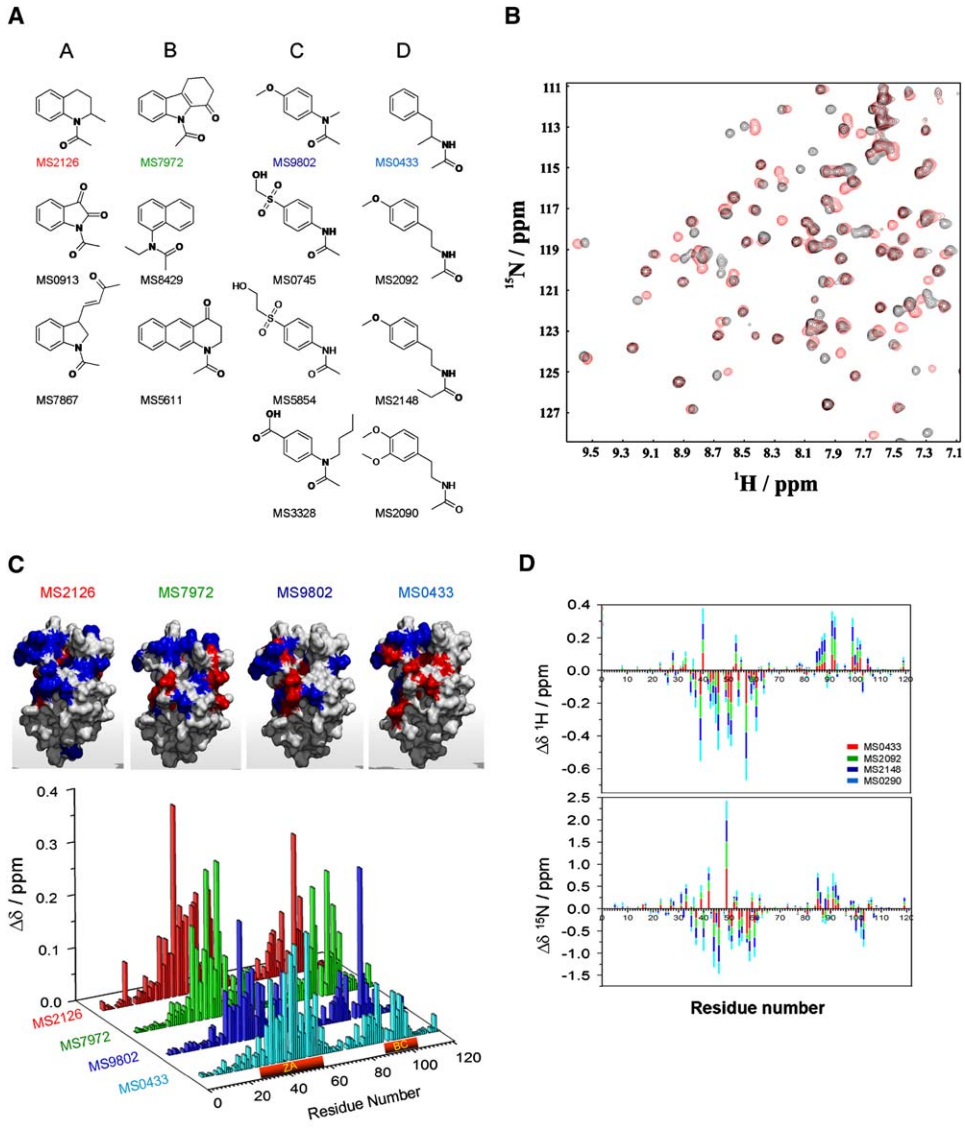

Figure 2. Discovery of Initial Lead Compounds for the CBP BRD

(A) Small-molecule compounds that bind to the CBP BRD.

(B) Superposition of 2D ^{1}H-^{15}N-HSQC spectra of the CBP BRD showing changes of the protein NMR resonances from the free form (black) to the complex form, with a representative compound, MS2126.

(C) Weighted ^{1}H and ^{15}N chemical shift changes ($\Delta\delta$) by the CBP BRD induced by binding to representative ligands from each group (i.e., MS2126, MS7972, MS9802, or MS0433). The AcK binding site lies between ZA and BC loops. Amino acid residues exhibiting major chemical shift perturbations are color-coded on the protein surface: red for 0.05 ppm < $\Delta\delta$ < 0.08 ppm; and blue for $\Delta\delta$ > 0.08 ppm. The orientation of the protein structure is similar to that in Figures 1A and 1B.

(D) Stack plot of absolute changes in chemical shift ($\Delta\delta^X = \delta^X_{+ligand} - \delta^X_{Free}$, where X is ^{1}H or ^{15}N) in the presence of four Group **D** compounds, along the ^{1}H or ^{15}N dimension. Note that directionality of chemical shift perturbations for each compound is the same.

presence and absence of screening mixture; positive mixtures were then deconvoluted to identify individual binding ligands. From this knowledge-based library, we have identified 14 compounds that bind to the CBP BRD (Figure 2A). All of these ligands (except the MS5611) showed selective binding to CBP BRD, as they did not show any binding to the structurally similar PCAF BRD (data not shown). A weighted chemical shift perturbation $\Delta\delta$,

$$\Delta\delta = \sqrt{\left(\delta^{1H}_{Complex} - \delta^{1H}_{Free}\right)^2 + \frac{1}{25}\left(\delta^{15N}_{Complex} - \delta^{15N}_{Free}\right)^2},$$

of protein residues was used to characterize small-molecule binding to the protein. As the protein residues that exhibited the most significant ligand-induced chemical shift perturbations are largely located in the ZA and BC loops (Figure 2C, lower panel), it is possible that all these compounds bind near the AcK binding site (Figure 2C, upper panel).

We classified these 14 compounds into 4 groups on the basis of their chemical structures (Figure 2A): (1) Group **A** compounds contain one aromatic ring fused to an alicyclic ring; (2) Group **B** compounds have two fused aromatic rings; (3) Group **C** compounds have

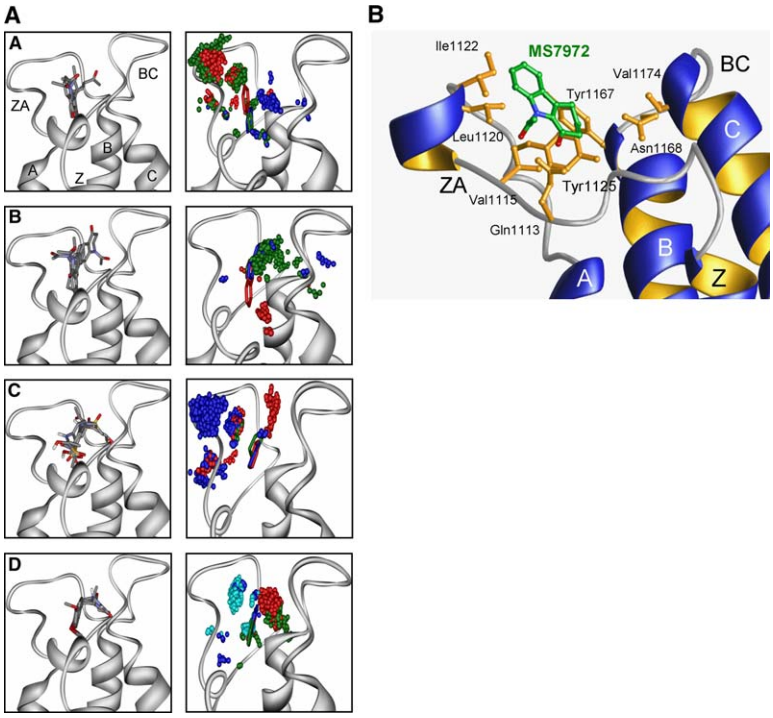

Figure 3. Structural Analysis of CBP BRD Interactions with Small Molecules

(A) Identification of binding locations of small molecules in the CBP BRD by Autodock 3.0 calculations (left panels) and J surface calculations using NMR chemical shift perturbation data at 2σ (right panels). Ribbons diagrams depict best binding modes of ligands of each group, as determined by Autodock 3.0 calculations. The aromatic ring of each compound is color-coded according to the corresponding J surface calculation.

(B) Three-dimensional structure of the CBP BRD bound to MS7972, as determined by NMR spectroscopy, illustrating the ligand binding site between the ZA and BC loops.

only one aromatic ring attached to a -$NHCOCH_3$ group; and (4) Group **D** compounds have one aromatic ring substituted with -$(CH_2)_2NHCOCH_3$.

The proper grouping of lead compounds provides valuable insights into structure-activity relationships (SAR) in their interaction with the CBP BRD. Consistent with their similarity in chemical structures, directionality of absolute changes in chemical shift perturbations along the ^1H or ^{15}N dimension in the 2D HSQC spectra was similar for compounds in a given group (e.g., Group **D** [Figure 2D]). Frequency of protein residues perturbed by different ligands in a given group highlights the importance of certain residues in ligand recognition (see Figure S1 in the Supplemental Data available with this article online). For example, there are 11 residues in the BRD, mostly located in the ZA or BC loop, perturbed by all the ligands in Group **A**. While overall residues perturbed by ligands crossing different groups are different, information of residues commonly perturbed by binding to different ligands can reveal similarity and/or difference in modes of ligand binding, and thus help in lead optimization. Taken together, these results indicate that the mode by which the protein interacts with ligands within one group is similar, thus justifying the classification of these compounds.

Identification of Ligand Binding Sites

Localization of ligand binding site in a target protein by chemical shift perturbation data alone is difficult, as a direct correlation between chemical shift perturbations and spatial proximity to a binding ligand can be masked by ligands with large shielding and anisotropies, as well as by effects of indirect conformational changes of the protein. Two alternative computational approaches can provide invaluable insights into the structural basis of protein/ligand recognition by localizing the ligand binding site in the target protein. First, computational docking calculation of 3D structure model of a ligand bound in a given target protein; the resulting structure model can be evaluated with chemical shift perturbation data obtained in NMR binding. Second, calculation of electron current density surface (J surface) [38]—a method that is based on the concept that the flow of electrons (J) is responsible for NMR chemical shifts and chemical shift perturbations.

Ligand docking into a target protein can be performed using Autodock 3.0 [39], which uses a genetic search algorithm as a global optimizer and energy minimization as a local search method. Although as a grid-based method, Autodock limits itself to a rigid model of a target protein, ligand flexibility is allowed. To predict the best docking mode for a given ligand, docking calculations generate a number of clusters (i.e., solutions with pairwise rmsd of all atoms of 1.0 Å) and rank of each docking mode (cluster rank). Docking mode is selected from the lowest-energy solution of a cluster corresponding to the minimum docking energy. The Autodock calculations show that the aromatic ring of almost all ligands is located in the hydrophobic AcK binding site (Figure 3A, left column). Most of the residues predicted to be interacting with ligands in the ZA and BC loops were also shown to be perturbed by NMR data. Notably, ligands that cause major chemical shift perturbations in the protein (i.e., "good binders") generate fewer clusters than ligands that cause minor chemical shift perturbations (i.e., "poor binders"), consistent with the notion that the former has a consensus of a single binding mode. While for a given ligand, ligand binding site in the BRD protein predicted by Autodock calculation generally correlates well with NMR chemical shift perturbation data, limitations of the docked structure models likely exist due to high mobility of the ZA and BC loops, as

assessed by the predicted NMR S^2 order parameters of $N\text{-}H^N$ vectors of the protein backbone amide that were calculated with its structure (Figure S2) [40]. Because the ZA and BC loops comprise the AcK binding site in the CBP BRD, such high structural dynamics may cause major conformational changes of the ligand binding site when bound to different ligands.

Calculation of J surface using chemical shift perturbation data can also help localize a ligand when bound to a target protein [38]. This method calculates the center of electron current density for a ligand aromatic ring using point-dipole that is represented as dot density (J surface), where the highest dot density correlates to the center of the ligand aromatic ring. The surface can, therefore, guide to locate the binding site for the aromatic ring of the ligand. When chemical shift perturbations are not caused by direct ligand binding, inconsistency between calculated J surface and chemical shift perturbation (i.e., diffused dot-density) may be observed. Possibly due to likely major conformational changes of the ZA and BC loops induced by ligand binding, many ligands from different groups show diffused dot-density (Figure 3A, right column). Nevertheless, the Group **B** ligands exhibit excellent consistency between calculated J surface and the observed chemical shift perturbation.

To validate the predicted ligand binding site for the Group **B** ligands, we solved the three-dimensional structure of the CBP BRD in complex with MS7972 (9-acetyl-2,3,4,9-tetrahydro-carbazol-1-one) by NMR. As revealed by the structure (Figure 3B, Table S1), the ligand is bound in a site formed by residues largely in the ZA loop at the entrance of the AcK binding pocket, confirming the computational prediction. Moreover, the structure also shows that the ligand forms a network of intermolecular hydrophobic and aromatic interactions with Val1115, Leu1120, Ile1122, Tyr1125, and Tyr1167, and that the acetyl and ketone groups with Val1115 and Leu1120, and Gln1113, respectively. Because many of these residues are involved in interactions with the p53-AcK382 peptide, binding of MS7972 to CBP BRD likely blocks the protein interaction with an AcK-containing binding partner, such as p53 (see below). Taken together, we show that combined use of NMR chemical shift perturbation mapping with Autodock and J surface calculations may rapidly establish the most probable structures of a protein bound to a ligand. Such model structures of protein/ligand complexes are important for rational design of pharmacophore and combinatorial libraries for lead improvement to optimize potency and ligand binding selectivity of initial leads for a specific target protein.

Inhibition of CBP BRD/p53-AcK382 Interactions by Lead Compounds

To evaluate whether these lead compounds are capable of blocking CBP BRD binding to lysine 382-acetylated p53, we performed an inhibition study. In this assay, a chemical ligand in a concentration-dependent manner competes against binding of the biotinylated p53-AcK382 peptide immobilized on streptavidin-agarose to the GST-fusion CBP BRD, as assessed by anti-GST Western blot. As shown in Figure 4A, while MS9802 and MS0433 showed relatively little inhibition activity against CBP BRD/p53-AcK382 association in a ligand

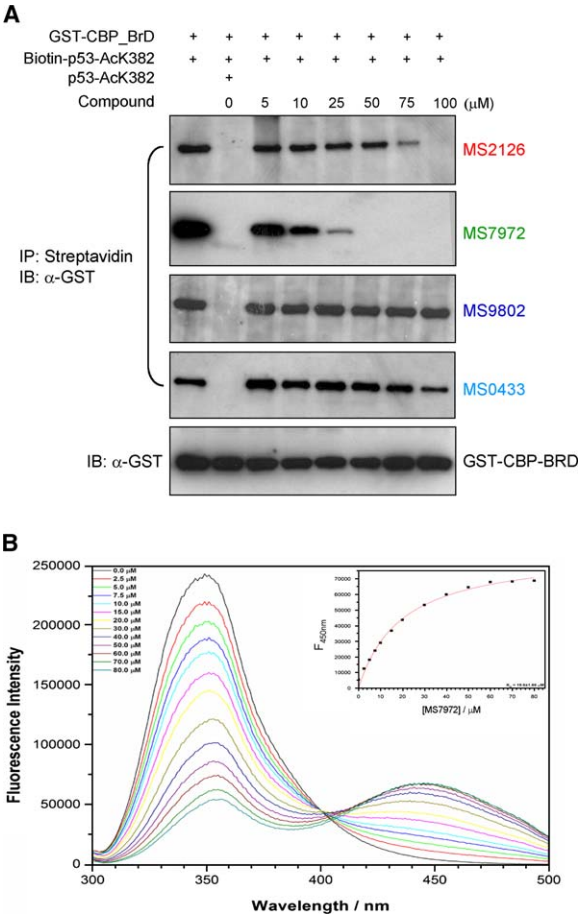

Figure 4. Small-Molecule Inhibition of CBP BRD and p53-AcK382 Interaction

(A) Inhibition of CBP BRD and p53-AcK382 peptide binding by lead compounds in a competition assay detected by anti-GST Western blot. In this assay, a lead compound competes against the biotinylated p53-AcK382 peptide that was immobilized on streptavidin-agarose beads for binding to the GST CBP BRD. Concentration of the biotinylated or the nonbiotinylated p53 peptide used in the assay is 10 μM and 25 μM, respectively, whereas compound concentration ranges from 0 to 100 μM, as indicated.

(B) Fluorescence titration of CBP BRD binding to MS7972. Superimposition of fluorescence spectra of the CBP BRD (~5 μM) with increasing amount of MS7972 (0–80 μM). Binding affinity was determined by monitoring fluorescence intensity change at 450 nm as a function of ligand concentration (inset).

concentration of 5–100 μM, MS2126 and MS7972 can almost completely block this BRD interaction at 100 μM and 50 μM, respectively. The inhibition activity of MS7972 is about 3-fold higher than that of MS2126. We further characterized binding affinity of the leading compound MS7972 binding to the protein using fluorescence spectroscopy. Of three tryptophan residues in this BRD, Trp1165 in the BC loop is nearest to the AcK binding site. The intrinsic tryptophan fluorescence shows emission maxima at 350 nm, indicating that the tryptophans are likely completely solvent-exposed. Addition of MS7972 to the CBP BRD results in emission at 445 nm and quenching of the CBP BRD due to resonance energy transfer (Figure 4B). Upon saturation with MS7972, the protein tryptophan fluorescence undergoes a red shift

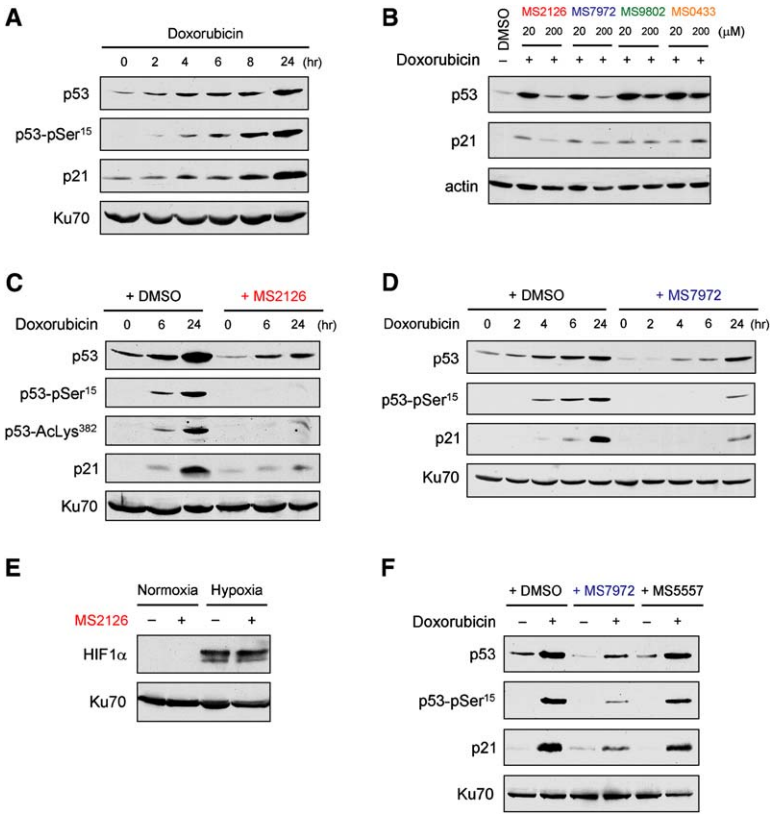

Figure 5. Modulation of p53 Function in Response to DNA Damage by Small Molecules

(A) Increased p53 expression in response to DNA damage agent doxorubicin treatment, as illustrated with U2OS cells. Wild-type p53-expressing U2OS cells were incubated with 0.1 μg/ml doxorubicin for the indicated time (up to 24 hr) and then subjected to immunoblotting analysis with specific antibodies.

(B) Small-molecule inhibition of the increase in p53 levels in response to DNA damage. Wild-type p53-expressing U2OS cells were either incubated with DMSO or treated with 20 or 200 μM of each small-molecule compound for 16 hr. Cells were then further incubated with 0.1 μg/ml doxorubicin for an additional 24 hr as shown. Cell lysates were then subjected to immunoblotting with the indicated antibodies.

(C and D) Modulation of p53 function in response to DNA damage by MS2126 or MS7972, respectively. Wild-type p53-expressing U2OS cells were either incubated with DMSO or treated with 200 μM of MS2126 or MS7972 for 16 hr. Cells were then further incubated with 0.1 μg/ml doxorubicin for the indicated times and then subjected to immunoblotting analysis with specific antibodies.

(E) Compound MS2126 does not affect the increase in HIF1α level in response to hypoxia. Wild-type p53-expressing U2OS cells were incubated in the absence or presence of 200 μM of MS2126 for 16 hr. Cells were then further incubated in either normoxic or hypoxic conditions for an additional 24 hr as shown. Cell lysates were then subjected to immunoblotting with the indicated antibodies.

(F) Compound MS5557 does not affect p53 function in response to DNA damage, as demonstrated in wild-type p53-expressing U2OS cells with experimental conditions similar to those in (C) and (D). The cells were treated with DMSO, MS7972 (200 μM), or MS5557 (200 μM) for 16 hr, and then further incubated with 0.1 μg/ml doxorubicin for 24 hr, and then subjected to immunoblotting analysis with specific antibodies.

at 350 nm, suggesting the possible change in protein local conformation upon ligand binding. Change of fluorescent intensity at 445 nm as a function of ligand concentration was used to determine binding constant, K_D, to be 19.6 ± 1.9 μM (mean ± SD), which is consistent with its inhibition activity (Figure 4A).

Modulation of p53 Function via Inhibition of p53/CBP Binding by Small Molecules

We assessed the effects of these initial lead compounds on p53 function as transcription activator in response to DNA damage in a cell-based assay. Consistent with what is reported in the literature, p53 expression in U2OS cells is low in a resting state, likely due to its negative regulation by Mdm2 through interaction with the N-terminal region of p53 (Figure 5A). Upon DNA damage stimulation by doxorubicin treatment, p53 becomes phosphorylated within the N-terminal activation domain including serine 15, relieving it from association with the negative regulator Mdm2 and resulting in p53 stabilization and an increase in protein level in the cell, as assessed by anti-p53 and anti-p53-pSer15 Western blots. In response to DNA damage, p53 also becomes acetylated on its C-terminal lysine residues including lysine 382, promoting its recruitment of the transcriptional coactivator CBP/p300 via BRD/AcK binding, which leads to histone acetylation and transcriptional activation of target genes, such as the cyclin-dependent kinase inhibitor p21 in cell cycle arrest [20, 23]. As shown in Figure 5B, treatment of U2OS cells with MS2126 or MS7972 at 200 μM, prior to the doxorubicin stimulation, results in a dramatic decrease of the doxorubicin-induced p53 increase as compared with the DMSO control. This is likely due to the possibility that the lysine-acetylated p53 in a free state is not stable in the cell, as it is subject to rapid deacetylation by histone deacetylases and subsequent ubiqutination and protein degradation by Mdm2 [21]. This effect is consistent with the corresponding decrease in p53-mediated p21 activation in response to doxorubicin-induced DNA damage. Treatment of U2OS cells with compound MS9802 or MS0433 showed much fewer effects, if any, on p53 protein level and activation in cells, which is consistent with their inability to inhibit CBP BRD/p53-AcK382 association in vitro (Figure 4A). Further studies at different time points after doxorubicin treatment show that treatment of MS2126 (Figure 5C) as well as MS7972 (Figure 5D) results in loss of p53 phosphorylation at Ser15 as well as acetylation at Lys382 (Figure 5C).

While generally in agreement, due to differences in chemical stability and cell permeability for individual compounds, the ligand concentration required for effects on p53 function in the cell-based assay appears higher than that for in vitro inhibition activity (Figure 4A). Although we cannot rule out possible effects of these compounds on other biological proteins in the cell, downregulation of p53 protein level and functional

activation in the presence of MS2126 or MS7972 that was exerted in a ligand concentration-dependent and doxorubicin exposure time-dependent manner likely result from their inhibitory activity in blocking CBP BRD/p53-AcK382 binding. Particularly, MS2126 does not seem to affect the upregulation of HIF1α under hypoxic conditions (Figure 5E), and MS5557, which is a structural analog of MS7972, but does not bind to the CBP BRD (Figure S3), does not modulate p53 function under DNA damage condition (Figure 5F), thus further highlighting the specificity of MS2126 and MS7972 for p53 function. Taken together, these results strongly suggest that inhibition of CBP BRD/p53 at AcK382 by small-molecule compounds can cause a dramatic inactivation of p53 transcriptional activity through promoting its protein instability by changes of its posttranslational modification states. Moreover, these cell-based assays provide a valuable assessment of cell permeability and in vivo efficacy of these small-molecule compounds on p53 function as a transcriptional activator for its target genes, which is essential for further lead optimization through SAR-guided chemical modifications.

Significance

Molecular mechanisms underlying p53 function that direct cellular responses to external stress signals are undoubtedly complex. Here, we show that small molecules designed to modulate specific molecular function of p53 can be used as powerful tools to explore mechanistic underpinnings of molecular interactions and regulation of p53 in physiological conditions. We also demonstrate that the knowledge of the structural and molecular basis of lysine 382-acetylated p53 interaction with the BRD of the coactivator CBP greatly facilitates our ability to identify small-molecule ligands for the target CBP BRD from NMR-based screening of a "focused" library constructed using a target structure-based approach. Our structure-based understanding of target interactions with different classes of the lead compounds lays a foundation for rational design of pharmacophore and chemical modifications for lead optimization of potency and binding selectivity. The emerging results from the cell-based study of p53 protein level and functional activation using these small molecules can feed back to the rational design to address issues of cell permeation and stability of lead chemicals. The approach reported here is applicable to rational design of small-molecule ligands for other protein modular domains that play an important role in regulation of a wide variety of cellular processes.

Experimental Procedures

Protein Sample Preparation

The BRD of CBP (residues 1082–1197) was expressed in *Escherichia coli* BL21(DE3) cells in the pET15b vector (Novagen, San Diego, CA), as described previously [23]. Isotope-labeled proteins were prepared from cells grown on a minimal medium containing $^{15}NH_4Cl$ with or without $^{13}C_6$-glucose in H_2O. The protein was purified by nickel-IDA affinity chromatography, followed by thrombin cleavage to remove an N-terminal poly-His-tag. GST-fusion BRD of CBP (residues 1082–1197) was expressed in *E. coli* in the pGEX4T3 vector (Amersham Biosciences Corp., Piscataway, NJ), and purified with a glutathione-sepharose column.

Chemical Screening by NMR Spectroscopy

All spectra were recorded at 25ºC on a Bruker 500 or 600 MHz NMR spectrometer. The NMR data were processed and analyzed using NMRPipe [41] and NMRView [42]. Typical protein solution for NMR study contained the CBP BRD of 0.2 mM in 100 mM phosphate buffer (pH 6.5), containing 5 mM perdeuterated DTT and 10% ^2H_2O. All chemical stocks were prepared at ~0.35 M in perdeuterated DMSO. Initial protein and compound binding by NMR was conducted with mixtures of eight compounds; each compound was 1–2 mM and deuterated DMSO was ~3% (v/v). The ligand binding was detected by observing ligand-induced chemical shift perturbations of residues of the ^{15}N-labeled protein recorded in 2D ^1H-^{15}N-HSQC spectra. The positive mixtures were deconvoluted by screening individual compounds to identify the active compound. Deuterated DMSO in the latter protein/ligand solution was ~0.8% (v/v), and a reference spectrum of the protein with DMSO alone with the corresponding concentration was collected for data analysis.

Protein Structure Determination by NMR

NMR samples contained the CBP BRD (0.5 mM) in complex with a chemical ligand, MS7972 (~2 mM), in 100 mM phosphate buffer (pH 6.5), containing 5 mM perdeuterated DTT and 0.5 mM EDTA in $H_2O/^2H_2O$ (9/1) or ^2H_2O. All NMR spectra were acquired at 30ºC on a Bruker 500 or 600 MHz NMR spectrometer. The backbone ^1H, ^{13}C, and ^{15}N resonances were assigned using 3D HNCACB and HN(CO)CACB spectra. The side-chain atoms were assigned from 3D HCCH-TOCSY and (H)C(CO)NH-TOCSY data. The NOE-derived distance restraints were obtained from ^{15}N- or ^{13}C-edited 3D NOESY spectra. The $^3J_{HN,H\alpha}$ coupling constants measured from 3D HNHA data were used to determine Φ-angle restraints. Slowly exchanging amide protons were identified from a series of 2D ^{15}N-HSQC spectra recorded after $H_2O/^2H_2O$ exchange. The intermolecular NOEs used in defining the structure of the CBP BRD/ligand complex were detected in ^{13}C-edited (F_1), $^{13}C/^{15}N$-filtered (F_3) 3D NOESY spectra [43]. Protein structures were calculated with a distance geometry-simulated annealing protocol with X-PLOR [44]. Initial structure calculations were performed with manually assigned NOE-derived distance restraints. Hydrogen-bond distance restraints, generated from the H/D exchange data, were added at a later stage of structure calculations for residues with characteristic NOEs. The converged structures were used for iterative automated NOE assignment by ARIA for refinement [45]. Structure quality was assessed by Procheck-NMR [46]. The structure of the protein/ligand complex was determined using intermolecular NOE-derived distance restraints.

Calculation of Electrostatic Potential

The DelPhi [47] program was used to calculate electrostatic potential by solving the linear form of the PBE. Manipulation of the potential map was done using the Delphi viewer module of UCSF Chimera [48] and Grasp [49]. The van der Waals radii and atomic charges were taken from the CHARMM22 parameter set. The program parameters used were as follows: interior dielectric, 2; exterior dielectric, 80; solvent probe radius, 1.4 Å; and ionic strength, 0.150 M.

Computational Docking

Docking of ligands to the CBP BRD was performed using AutoDock v3.0.5 [39], which uses a genetic algorithm as a global optimizer combined with energy minimization as a local search method. In this method, the target protein is kept to be rigid and represented as a grid, while torsional flexibility is allowed in the ligand. Mass-centered (blind-docking) as well as binding-site-centered affinity grid maps were generated with 0.375 Å spacing using the Autogrid program for the protein target. Blind-docking was used to evaluate the accuracy of prediction of correct binding site, which was determined based on NMR binding results. The Lamarckian genetic algorithm (LGA) and pseudo-Solis and Wets method were used for minimization. Default parameters for Autodock calculations were used, except for what is otherwise stated. Particularly, for blind-docking, each grid map consisted of a 126 × 126 × 126 grid, with the center of the map assigned to the geometric center of the protein. Each LGA job consisted of 50 runs with 270,000 generations in each run

and maximum number of energy evaluations set to 2.5×10^6. Moreover, for binding-site-centered docking, a $62 \times 76 \times 80$ grid was generated with each LGA job that consisted of 200 runs with 270,000 generations in each run and maximum number of energy evaluations of 5.0×10^6. Resulting docked orientations within 1.0 Å rmsd tolerance of each other were clustered together. Docked conformations were analyzed using AutoDockTools (http://www.scripps.edu/~sanner) and LIGPLOT [50].

Structures of chemical ligands were generated using molecular modeling software SYBYL v6.7 (Tripos Associated, Inc., St. Louis, MO). Partial atomic charges were assigned using the Gasteiger-Marsili method [51]. The program Autotors was used to define torsional degrees of freedom in ligands. All the possible torsions were allowed. The coordinates used in the Autodock calculation were taken from the first model of NMR structures of CBP BRD/p53-AcK382 peptide complex (PDB 1JSP) [23]. For the docking purpose, the peptide coordinates were removed. Kollman united-atom partial charges and solvation parameters were added to the protein file using AutoDockTools.

J Surface Calculation

J surface calculation was performed using the program Jsurf, originally developed by McCoy and coworkers [38] and latter modified and kindly provided by G. Moyna (The University of the Sciences, Philadelphia, PA). This program quantifies effect of spatial dependence of aromatic ring current field (from a ligand) on local magnetic fields of neighboring spins at the ligand binding site within the target protein. Assuming chemical shift perturbation observed at a protein proton i, Δ_i, where $\Delta_i = \delta^i_{bound} - \delta^i_{free}$, is generated mainly by aromatic ring current effect from the ligand; the origin of Δ_i can be approximated by a single-point dipole located at the center of the ligand aromatic ring, and therefore $\Delta_i = \delta^i_{bound} - \delta^i_{free} \approx \left(\frac{B_{dip}}{R_i^3}\right)\left(1 - 3\cos^2\theta_i\right)$, where R_i is the length of the vector from the center of the ligand ring to the perturbed protein atom i, θ_i is the angle between the ring plane normal and R_i, and B_{dip} is a proportionality constant. The calculation of J surface requires an input file containing absolute change in chemical shift for backbone amide proton of perturbed residues. Only residues with $\Delta \geq |0.05|$ were used for the calculation. The Δ_i information was translated into the ligand localization using spherical dot density representation, done by the program Jsurf.

MD Simulation

MD simulation of the CBP BRD was done using Gromacs 3.2.1 [52] and GROMOS96 (v. 43a1) force field [53]. As starting geometry, the first model of NMR structures of the CBP BRD (PDB 1JSP; without the peptide) was used. The protein was centered in a periodic cubic simulation box with a minimum protein-box distance of 1.0 nm and a volume of 351.03 nm^3. The box was filled with 10,969 SPC water molecules [54]. One Na^+ was added to ensure charge neutrality of the simulation cell. The MD protocol used the LINCS method [55] to constrain covalent bond lengths. Temperature and pressure were kept constant separately by coupling the protein, ions, and solvent to external temperature and pressure baths with the respective coupling constant (τ) of 0.1 ps and 0.5 ps. The reference temperature was adjusted to 300 K. To relax the solvent configuration, a steepest descent minimization was adopted. The following step was position-restrained dynamics, which restrains atom positions of the protein while letting the solvent move in the simulation box to reach equilibrium before a full molecular dynamics simulation starts. Long-range electrostatics was calculated with the Particle-Mesh Ewald (PME) method [56, 57]. The MD time step was set at 0.002 ps. After equilibration, the simulation time used was 5 ns.

Estimation of Backbone Amide S^2 Order Parameters from the Protein Structure

The S^2 order parameter of protein backbone amide vectors was calculated from the protein 3D structure using an analytical relationship [40]. The method relates S^2 of amide vector of residue i to close contacts experienced by the amide proton and carbonyl oxygen of the preceding residue i-1 with heavy atoms k:

$$S_i^2 = \tanh\left(2.656\sum_k\left(\exp\left(-r^O_{i-1,k}/1\text{Å}\right)\right) + 0.8\left(\exp\left(-r^H_{i,k}/1\text{Å}\right)\right)\right) + b$$

where $r^O_{i-1,k}$ is the distance from the carbonyl oxygen of residue i-1 to the heavy atom k, and $r^H_{i,k}$ is the distance between the amide proton and the heavy atom k. The parameter b was set to −0.1, considering that the value of order parameter for rigid protein region typically is about 0.9. A python-based script that uses MMTK [58] was used for the calculation (http://nmr.clarku.edu/software/S2/s2predict.html).

Fluorescence Binding Experiment

Fluorescence measurements were performed on an ISS PC1 photon-counting spectrofluorometer at room temperature. The concentration of the protein (calculated using the theoretical absorption coefficient of 24,750 $M^{-1}cm^{-1}$ at 280 nm) was 5 μM in 100 mM phosphate buffer (pH 6.5) containing 5 mM DTT. Protein intrinsic fluorescence was measured at an excitation wavelength of 295 nm, and emission was collected from 300–500 nm using 8 nm band passes for both excitation and emission. The protein sample was titrated with a ligand MS7972, to a final concentration of 80 μM with 0.7% final dilution.

In Vitro Protein-Peptide Binding Assay

GST-fusion CBP BRD (10 μM) was incubated with an N-terminal biotinylated p53 AcK382 peptide (50 μM) in a 50 mM Tris buffer (pH 7.5), containing 50 mM NaCl, 0.1% BSA, and 1 mM DTT, at 22ºC for 2 hr. Streptavidin-agarose beads were added to the mixture and washed in the Tris buffer containing 500 mM NaCl and 0.1% NP-40. The CBP BRD eluted from the beads was run on SDS-PAGE, and visualized in Western blots by anti-GST antibody and horseradish peroxidase-conjugated goat anti-rabbit IgG. Small-molecule inhibition assay was performed by incubating the CBP BRD and the biotinylated p53 AcK382 peptide with increasing amounts of small-molecule compound.

p53 Expression and Functional Assays

Wild-type p53-expressing U2OS cells were either incubated with DMSO or treated with 20 or 200 μM of various small-molecule compounds for about 16 hr. The cells were further incubated with 0.1 μg/ml doxorubicin for a specified time of 2 to 24 hr, and then cell lysates were subjected to immunoblotting analysis using specific antibodies for p53, phosphorylated Ser15 of p53, acetylated Lys382 of p53, p21, or Ku70. For the upregulation of HIF1α, U2OS cells were incubated in the absence or presence of 200 μM of MS2126 for 16 hr, and then further incubated in either normoxic or hypoxic conditions for an additional 24 hr. Cell lysates were then subjected to immunoblotting with the specific antibodies for HIF1α and Ku70.

Supplemental Data

Supplemental Data, including Table S1 and Figures S1–S3, are available at http://www.chembiol.com/cgi/content/full/13/1/81/DC1/.

Acknowledgments

We thank Dr. G. Moyna for providing the Jsurf program and technical advice. S. is a recipient of the American Foundation for AIDS Research Postdoctoral Fellowship. J.M. and M.-M.Z. are supported by grants from the National Institutes of Health.

Received: February 26, 2005
Revised: September 27, 2005
Accepted: October 26, 2005
Published: January 20, 2006

References

1. Vousden, K.H., and Lu, X. (2002). Live or let die: the cell's response to p53. Nat. Rev. Cancer *2*, 594–604.
2. Oren, M. (2003). Decision making by p53: life, death and cancer. Cell Death Differ. *10*, 431–442.
3. el-Deiry, W.S. (1998). Regulation of p53 downstream genes. Semin. Cancer Biol. *8*, 345–357.
4. Vogelstein, B., Lane, D., and Levine, M.J. (2000). Surfing the p53 network. Nature *408*, 307–310.
5. Levine, A.J. (1997). p53, the cellular gatekeeper for growth and division. Cell *88*, 323–331.

6. Prives, C., and Hall, P.A. (1999). The p53 pathway. J. Pathol. *187*, 112–126.
7. Ko, L.J., and Prives, C. (1996). p53: puzzle and paradigm. Genes Dev. *10*, 1054–1072.
8. Alarcon-Vargas, D., and Ronai, Z. (2002). p53-Mdm2: the affair that never ends. Carcinogenesis *23*, 541–547.
9. Haupt, Y., Maya, R., Kazaz, A., and Oren, M. (1997). Mdm2 promotes the rapid degradation of p53. Nature *387*, 296–299.
10. Kubbutat, M.H., Jones, S.N., and Vousden, K.H. (1997). Regulation of p53 stability by Mdm2. Nature *387*, 299–303.
11. Momand, J., and Zambetti, G.P. (1997). Mdm-2: "big brother" of p53. J. Cell. Biochem. *64*, 343–352.
12. Hupp, T.R., and Lane, D.P. (1994). Allosteric activation of latent p53 tetramers. Curr. Biol. *4*, 865–875.
13. Wang, Y., and Prives, C. (1995). Increased and altered DNA binding of human p53 by S and G2/M but not G1 cyclin-dependent kinases. Nature *376*, 88–91.
14. Sakaguchi, K., Herrera, J.E., Saito, S., Miki, T., Bustin, M., Vassilev, A., Anderson, C.W., and Appella, E. (1998). DNA damage activates p53 through a phosphorylation-acetylation cascade. Genes Dev. *12*, 2831–2841.
15. Gu, W., and Roeder, R.G. (1997). Activation of p53 sequence-specific DNA binding by acetylation of the p53 C-terminal domain. Cell *90*, 595–606.
16. Liu, L., Scolnick, D.M., Trievel, R.C., Zhang, H.B., Marmorstein, R., Halazonetis, T.D., and Berger, S.L. (1999). p53 sites acetylated in vitro by PCAF and p300 are acetylated in vivo in response to DNA damage. Mol. Cell. Biol. *19*, 1202–1209.
17. Ito, A., Lai, C.H., Zhao, X., Saito, S., Hamilton, M.H., Appella, E., and Yao, T.P. (2001). p300/CBP-mediated p53 acetylation is commonly induced by p53-activating agents and inhibited by MDM2. EMBO J. *20*, 1331–1340.
18. Luo, J., Su, F., Chen, D., Shiloh, A., and Gu, W. (2000). Deacetylation of p53 modulates its effect on cell growth and apoptosis. Nature *408*, 377–381.
19. Guo, A., Salomoni, P., Luo, J., Shih, A., Zhong, S., Gu, W., and Pandolfi, P.P. (2000). The function of PML in p53-dependent apoptosis. Nat. Cell Biol. *2*, 730–736.
20. Barlev, N.A., Liu, L., Chehab, N.H., Mansfield, K., Harris, K.G., Halazonetis, T.D., and Berger, S.L. (2001). Acetylation of p53 activates transcription through recruitment of coactivators/histone acetyltransferases. Mol. Cell *8*, 1243–1254.
21. Li, M., Luo, J., Brooks, C.L., and Gu, W. (2002). Acetylation of p53 inhibits its ubiquitination by Mdm2. J. Biol. Chem. *277*, 50607–50611.
22. Pearson, M., Carbone, R., Sebastiani, C., Cioce, M., Fagioli, M., Saito, S., Higashimoto, Y., Appella, E., Minucci, S., Pandolfi, P.P., et al. (2000). PML regulates p53 acetylation and premature senescence induced by oncogenic Ras. Nature *406*, 207–210.
23. Mujtaba, S., He, Y., Zeng, L., Yan, S., Plotnikova, O., Sachchidanand, Sanchez, R., Zeleznik-Le, N.J., Ronai, Z., and Zhou, M.-M. (2004). Structural mechanism of the bromodomain of the coactivator CBP in p53 transcriptional activation. Mol. Cell *13*, 251–263.
24. Shuker, S.B., Hajduk, P.J., Meadows, R.P., and Fesik, S.W. (1996). Discovering high-affinity ligands for proteins: SAR by NMR. Science *274*, 1531–1534.
25. Hajduk, P.J., Meadows, R.P., and Fesik, S.W. (1997). Discovering high-affinity ligands for proteins. Science *278*, 498–499.
26. Hajduk, P.J., Meadows, R.P., and Fesik, S.W. (1999). NMR-based screening in drug discovery. Q. Rev. Biophys. *32*, 211–240.
27. Moore, J.M. (1999). NMR screening in drug discovery. Curr. Opin. Biotechnol. *10*, 54–58.
28. Lepre, C.A. (2001). Library design for NMR-based screening. Drug Discov. Today *6*, 133–140.
29. Gorse, D., Rees, A., Kaczorek, M., and Lahana, R. (1999). Molecular diversity and its analysis. Drug Discov. Today *4*, 257–264.
30. Martin, E.J., and Critchlow, R.E. (1999). Beyond mere diversity: tailoring combinatorial libraries for drug discovery. J. Comb. Chem. *1*, 32–45.
31. Zeng, L., and Zhou, M.M. (2002). Bromodomain: an acetyl-lysine binding domain. FEBS Lett. *513*, 124–128.
32. Winston, F., and Allis, C.D. (1999). The bromodomain: a chromatin-targeting module? Nat. Struct. Biol. *6*, 601–604.
33. Marmorstein, R., and Berger, S.L. (2001). Structure and function of bromodomains in chromatin-regulating complexes. Gene *272*, 1–9.
34. Dhalluin, C., Carlson, J.E., Zeng, L., He, C., Aggarwal, A.K., and Zhou, M.M. (1999). Structure and ligand of a histone acetyltransferase bromodomain. Nature *399*, 491–496.
35. Mujtaba, S., He, Y., Zeng, L., Farooq, A., Carlson, J.E., Ott, M., Verdin, E., and Zhou, M.M. (2002). Structural basis of lysine-acetylated HIV-1 Tat recognition by PCAF bromodomain. Mol. Cell *9*, 575–586.
36. Owen, D.J., Ornaghi, P., Yang, J.C., Lowe, N., Evans, P.R., Ballario, P., Neuhaus, D., Filetici, P., and Travers, A.A. (2000). The structural basis for the recognition of acetylated histone H4 by the bromodomain of histone acetyltransferase gcn5p. EMBO J. *19*, 6141–6149.
37. Lipinski, C.A., Lombardo, F., Dominy, B.W., and Feeney, P.J. (1997). Experimental and computational approaches to estimate solubility and permeability in drug discovery and development settings. Adv. Drug Deliv. Rev. *23*, 3–25.
38. McCoy, M.A., and Wyss, D.F. (2002). Spatial localization of ligand binding sites from electron current density surfaces calculated from NMR chemical shift perturbations. J. Am. Chem. Soc. *124*, 11758–11763.
39. Morris, G.M., Goodsell, D.S., Halliday, R.S., Huey, R., Hart, W.E., Belew, R.K., and Olson, A.J. (1998). Automated docking using a Lamarckian genetic algorithm and an empirical binding free energy function. J. Comput. Chem. *19*, 1639–1662.
40. Zhang, F., and Bruschweiler, R. (2002). Contact model for the prediction of NMR N-H order parameters in globular proteins. J. Am. Chem. Soc. *124*, 12654–12655.
41. Delaglio, F., Grzesiek, S., Vuister, G.W., Zhu, G., Pfeifer, J., and Bax, A. (1995). NMRPipe: a multidimensional spectral processing system based on UNIX pipes. J. Biomol. NMR *6*, 277–293.
42. Johnson, B.A., and Blevins, R.A. (1994). NMR View: a computer-program for the visualization and analysis of NMR data. J. Biomol. NMR *4*, 603–614.
43. Clore, G.M., and Gronenborn, A.M. (1994). Multidimensional heteronuclear nuclear magnetic resonance of proteins. Meth. Enzymol. *239*, 349–363.
44. Brunger, A.T. (1993). X-PLOR Version 3.1: A system for X-Ray Crystallography and NMR, Version 3.1 (New Haven, CT: Yale University Press).
45. Nilges, M., and O'Donoghue, S. (1998). Ambiguous NOEs and automated NOE assignment. Prog. NMR Spectroscopy *32*, 107–139.
46. Laskowski, R.A., Rullmannn, J.A., MacArthur, M.W., Kaptein, R., and Thornton, J.M. (1996). AQUA and PROCHECK-NMR: programs for checking the quality of protein structures solved by NMR. J. Biomol. NMR *8*, 477–486.
47. Nicholls, A., and Honig, B. (1991). A rapid finite-difference algorithm, utilizing successive over-relaxation to solve the Poisson-Boltzmann equation. J. Comput. Chem. *12*, 435–445.
48. Pettersen, E., Goddard, T., Huang, C., Couch, G., Greenblatt, D., Meng, E., and Ferrin, T. (2004). UCSF chimera: a visualization system for exploratory research and analysis. J. Comput. Chem. *25*, 1605–1612.
49. Nicholls, A., Bharadwj, R., and Honig, B. (1993). GRASP: graphical representation and analysis of surface properties. Biophys. J. *64*, 166–170.
50. Wallace, A.C., Laskowski, R.A., and Thornton, J.M. (1995). LIGPLOT: a program to generate schematic diagrams of protein-ligand interactions. Protein Eng. *8*, 127–134.
51. Gasteiger, J., and Marsili, M. (1980). Iterative partial equalization of orbital electronegativity: a rapid access to atomic charges. Tetrahedron *36*, 3219–3228.
52. Lindahl, E., Hess, B., and van der Spoel, D. (2001). GROMACS 3.0: a package for molecular simulation and trajectory analysis. J. Mol. Model. *7*, 306–317.
53. van Gunsteren, W.F., Billeter, S.R., Eising, A.A., Hünenberger, P.H., Krüger, P., Mark, A.E., Scott, W.R.P., and Tironi, I.G. (1996). The GROMOS96 Manual and User Guide (Zurich, Switzerland: Hochschulverlag AG an der ETH Zurich).

54. Berendesen, H.J.C., Postma, J.P.M., van Gunsteren, W.F., and Hermans, J. (1981). Intermolecular Forces (Dordrecht, The Netherlands: Reidel).
55. Hess, B., Bekker, H., Berendsen, H.J.C., and Fraaije, J. (1997). LINCS: A linear constraint solver for molecular simulations. J. Comput. Chem. *18*, 1463–1472.
56. Essmann, U., Perera, L., Berkowitz, M.L., Darden, T., Lee, H., and Pedersen, L.G. (1995). A smooth particle mesh ewald method. J. Chem. Phys. *103*, 8577–8593.
57. Darden, T., York, D., and Pedersen, L. (1993). Particle mesh Ewald: an N.Log(N) method for Ewald sums in large systems. J. Chem. Phys. *98*, 10089–10092.
58. Hinsen, K. (2000). The molecular modeling toolkit: a new approach to molecular simulations. J. Comput. Chem. *21*, 79–85.

Accession Numbers

Coordinates have been deposited in the Protein Data Bank with accession code 2D82.